RESEARCH ARTICLE SUMMARY

CARBON CYCLE

Hidden comet tails of marine snow impede ocean-based carbon sequestration

Rahul Chajwa, Eliott Flaum, Kay D. Bidle, Benjamin Van Mooy, Manu Prakash*

INTRODUCTION: Phytoplankton in the upper layer of the ocean agglomerates and sinks under gravity, giving rise to a natural carbon transport mechanism termed "biological pump." The perpetual shower of soft and fragile marine snow in the ocean is estimated to be annually sequestering 2 to 4.5 billion tons of carbon from the atmosphere into the abyss, regulating both the atmospheric carbon dioxideand the sustenance of marine ecosystems. A predictive underpinning of marine snow is thus crucial. However, we currently lack a quantitative microphysics-based framework for the formation, sedimentation, and remineralization of marine snow, leading to major uncertainties in the current carbon flux estimates in climate models.

RATIONALE: Because sedimentation physics is at the heart of marine snow phenomena, we took an observation-driven approach to addressing this problem. Based on the 19th-century paradigm of Stokes' law and its ad hoc generalizations, researchers had been seeking a universal trend in how size is related to sinking speed in marine snow. Because marine snow is a structurally complex soft matter that deforms while sinking under its own weight, it violates key assumptions underlying Stokes' law and presents a classic two-way fluid-structure coupling that remained unexplored. To directly investigate the sinking dynamics of this complex object, we organized an ocean expedition (Cruise ID: EN667) during an algal bloom in the Gulf of Maine (42.5°N, 69.5°W). Marine snow aggregates were collected through freely hanging sediment traps in multiple deployments at a depth of 80 m. To directly observe sedimentation dynamics of these aggregates at sea, we utilized a new scale-free vertical tracking microscope mounted on a two-axis gimbal that minimized mechanical noise from ship's motion and allowed us to track small aggregate (equivalent spherical diameter < 750 μm) sinking over long times. To visualize the flow around sinking aggregates, we used a tracer bead (diameter 700 nm to 2 μm) solution.

RESULTS: By directly measuring the sinking velocities and detailed flows around individual marine snow particles, we discovered a new morphological feature in marine snow: a physical invisible comet tail forming a halo around a visible particulate matter during sedimentation. These hitherto-unseen comet tails are made of viscoelastic transparent exopolymer, which fundamentally modifies the sinking behavior. Our observations guided a new theoretical framework based on Stokesian sedimentation in which we included this previo invisible degree of freedom and construct reduced-order model for these compound particles. Furthermore, the combination of field experiments and theory enabled a sedimentation-based measurement of the elastic response of the mucus. We corroborated these findings with three-dimensional volumetric imaging of marine snow particles, which illuminate the heterogeneous microstructure of marine snow.

CONCLUSION: Through detailed analysis of more than 100 marine snow aggregates studied individually, we discovered hidden comet tails that effectively act as "physical" drag lines on sinking marine snow. This mucus-induced impedance almost doubles the estimate of mean residence time of marine snow in the Euphotic zone, nearly halting some particles to a standstill. This suggests a substantial overestimate in the flux inferred by using only the visible size of a marine snow particle. The discovery of multiphase nature of marine snow and a new conceptual framework that incorporates the invisible degrees of freedom in the sedimentation dynamics lays the foundation for understanding the formation, sedimentation, and remineralization of marine snow in the purview of physics. The crucial role of viscoelasticity of marine mucus as one of the knobs of carbon flux opens rich possibilities for studying biological origin of mucus and its complex rheology in the open oceans and potential biogeoengineering remediation. ■

The list of author affiliations is available in the full article online.
*Corresponding author. Email: manup@stanford.edu
Cite this article as R. Chajwa *et al.*, *Science* **386**, eadl5767 (2024). DOI: 10.1126/science.adl5767

READ THE FULL ARTICLE AT
https://doi.org/10.1126/science.adl5767

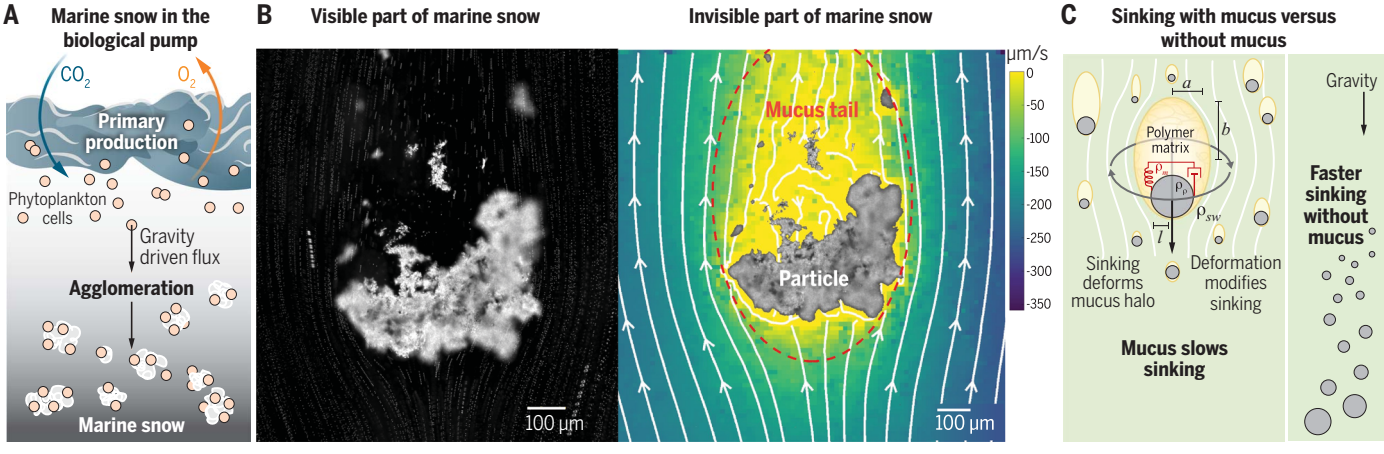

Hidden comet tails of marine snow. (**A**) A simplified depiction of carbon sequestration in the biological pump through marine snow. (**B**) Experimental data: (Left) Image of sinking marine snow visualized with tracer beads in the background and (right) fluid flow corresponding to the same particle showing the invisible mucus tail (yellow region) that falls along with the particle, greatly increasing the particle's effective size. (**C**) Impact of mucus on sedimentation: Mucus greatly increases the time marine snow can spend in the upper layers of the ocean, presenting a natural knob in this carbon flux. ρ_m, mucus density; ρ_{sw}, sea water density; ρ_p, particulate density; *a*, semiminor axis of the mucus comet tail; *b*, semimajor axis of the mucus comet tail; *l*, size of the visible aggregate.

RESEARCH ARTICLE

CARBON CYCLE

Hidden comet tails of marine snow impede ocean-based carbon sequestration

Rahul Chajwa[1], Eliott Flaum[1,2], Kay D. Bidle[6], Benjamin Van Mooy[7], Manu Prakash[1,3,4,5]*

Gravity-driven sinking of "marine snow" sequesters carbon in the ocean, constituting a key biological pump that regulates Earth's climate. A mechanistic understanding of this phenomenon is obscured by the biological richness of these aggregates and a lack of direct observation of their sedimentation physics. Utilizing a scale-free vertical tracking microscopy in a field setting, we present microhydrodynamic measurements of freshly collected marine snow aggregates from sediment traps. Our observations reveal hitherto-unknown comet-like morphology arising from fluid-structure interactions of transparent exopolymer halos around sinking aggregates. These invisible comet tails slow down individual particles, greatly increasing their residence time. Based on these findings, we constructed a reduced-order model for the Stokesian sedimentation of these mucus-embedded two-phase particles, paving the way toward a predictive understanding of marine snow.

Our oceans are the most dominant open reservoir and sink of carbon on our planet (*1*) and have absorbed roughly 30% of the anthropogenically released carbon dioxide since industrialization (*2*). A fraction of the carbon absorbed by the ocean is transported to depth and sequestered in the ocean sediments (*3*, *4*) by a process commonly called "biological pump" (*5*–*7*). This process, the result of photosynthesis in the upper sunlit layer of the ocean and the subsequent gravitationally driven sinking of organic matter, called "marine snow" (*8*–*13*), decouples the atmosphere from the deep ocean for timescales ranging from millennial to geological in duration (*5*, *14*). The challenge of studying these highly heterogeneous aggregates arises from their biological richness and physical complexity. Every marine snow particle is biologically singular, with plethora of planktonic species (both living and nonliving) and an associated bacterial and viral ecosystem (*15*). Furthermore, a process of sedimentation-driven self-assembly builds the aggregate through cellular adhesion, forming a specific kind of fragile soft matter. These biological and physical processes are in continuous feedback with each other, encompassing multiple length- and timescales (Fig. 1, A and B) (*8*, *16*). Thus, although vital to our understanding of current and future climate, the lack of predictive understanding of marine snow sedimentation (*17*, *18*) manifests itself as major uncertainty in current climate model (*19*, *20*).

Quantitative measurements of total amount of material collected in a sedimentation trap (a common method used to catch marine snow) across various depths in the ocean have highlighted the dramatic reduction in organic matter flux as a function of depth in our oceans (*3*), giving an empirical relationship called the Martin curve (*3*). In situ sedimentation (*22*–*30*) and UVP imaging (*27*, *31*) of marine snow along with the Martin curve (*3*) has allowed meaningful estimates of carbon flux in the ocean (*18*, *32*). Although widely utilized in our current climate models (*33*), the microscopic origin of this empirical curve remains largely unknown, and its universality remains speculative (*33*, *34*). In addition to bearing the uncertainties associated with the Martin curve (*18*, *33*), these flux calculations rely on a priori knowledge of the density-to-drag ratio (*35*) while assuming that "visible" size is sufficient to capture the structural complexity of marine snow. This invokes the long-standing puzzle in the sedimentation of marine snow (*32*, *36*).

A single phytoplankton cell, such as a diatom, owing to its small size and relative density, would take about a year to reach the bottom of the ocean, even if it were to continuously sink. Agglomeration of living matter owing to cell-cell adhesion (*16*, *21*) greatly increases the sinking speed of the resulting aggregate by an order of magnitude (*37*) owing to increased size (*38*) and reduced drag (*39*). In addition, zooplankton can both disintegrate (*40*) and compact these particles into fecal pellets (*41*), thus modifying their sinking speeds. Bacterial degradation further alters the physical characteristics of these particles (*42*, *43*). It is well known that marine snow particles contain transparent exopolymer particles (TEP) (*44*), previously implicated in aggregation models to impact the flocculation of diatom and cocolithopore blooms (*16*, *44*–*46*); however, the role of this mucus in the sedimentation dynamics of marine snow has been obscure. All the above dynamical processes in concert makes marine snow an enigmatic phenomenon with a rich sedimentation physics.

Owing to the paramount importance of these particles, various past attempts have been made to decipher their size-sinking relationship (*18*, *32*) and to quantify their biochemical (*47*) and physical nature (*13*, *48*). Conventional field observations made by using sediment traps (*3*) gives bulk estimates of the exported carbon, whereas in-situ underwater measurements through SCUBA (*22*–*24*), underwater imaging (*25*–*27*), with vertical settling columns (*28*), sediment trap (*29*), and gel trap (*30*), have provided valuable insights into the size, shape, and sinking statistics (*18*, *36*, *48*–*50*), but a one-to-one structure-sedimentation map of marine snow remains elusive (*32*). Because the processes central to the formation, sinking, and remineralization of marine snow occur at microscopic scales in the upper layer of the ocean, wider calls have been made previously to highlight this gap in our understanding of marine snow (*17*, *21*).

We approach the central issue of sedimentation of this material by fusing the classic sediment trap sampling (*3*, *51*) with the state-of-the-art scale-free vertical tracking microscopy called Gravity Machine (GM) (*52*). In this study, through a combination of ocean expedition and table-top experiments conducted on a research vessel, we elucidate a new morphological feature of sinking marine snow: an invisible comet tail forming a halo around visible particulate matter during sedimentation. Through direct imaging, we present a multiscale dataset of sedimentation dynamics of marine snow, observed at submicrometer resolution falling over a meter scale. This was done by collecting marine snow particles at a depth of 80 m and immediately measuring their sedimentation dynamics on board a research vessel, making it the largest database of flow microscopy of an untethered sinking marine snow aggregate, with sizes ranging from 0.1 to 0.7mm. Particle image velocimetry (PIV) analysis of this dataset revealed a hidden and almost universal feature of mucus comet tails in these sinking particles. We show that this hitherto-unseen invisible part of marine snow, which is largely made of a viscoelastic TEP, fundamentally modifies its sedimentation dynamics. These hidden comet tails effectively act as a "physical" drag line on sinking particles, bringing some particles to an almost standstill. Next, we present a reduced-order model for the fluid-structure interaction and

[1]Department of Bioengineering, Stanford University, Stanford, CA 94305, USA. [2]Graduate Program in Biophysics, Stanford University, Stanford, CA 94305, USA. [3]Department of Biology, Stanford University, Stanford, CA 94305, USA. [4]Department of Ocean, Stanford University, Stanford, CA 94305, USA. [5]Woods Institute for the Environment, Stanford University, Stanford, CA 94305, USA. [6]Department of Marine and Coastal Science, Rutgers University, New Brunswick, NJ 08901, USA. [7]Woods Hole Oceanographic Institution, Woods Hole, MA, USA.
*Corresponding author. Email: manup@stanford.edu

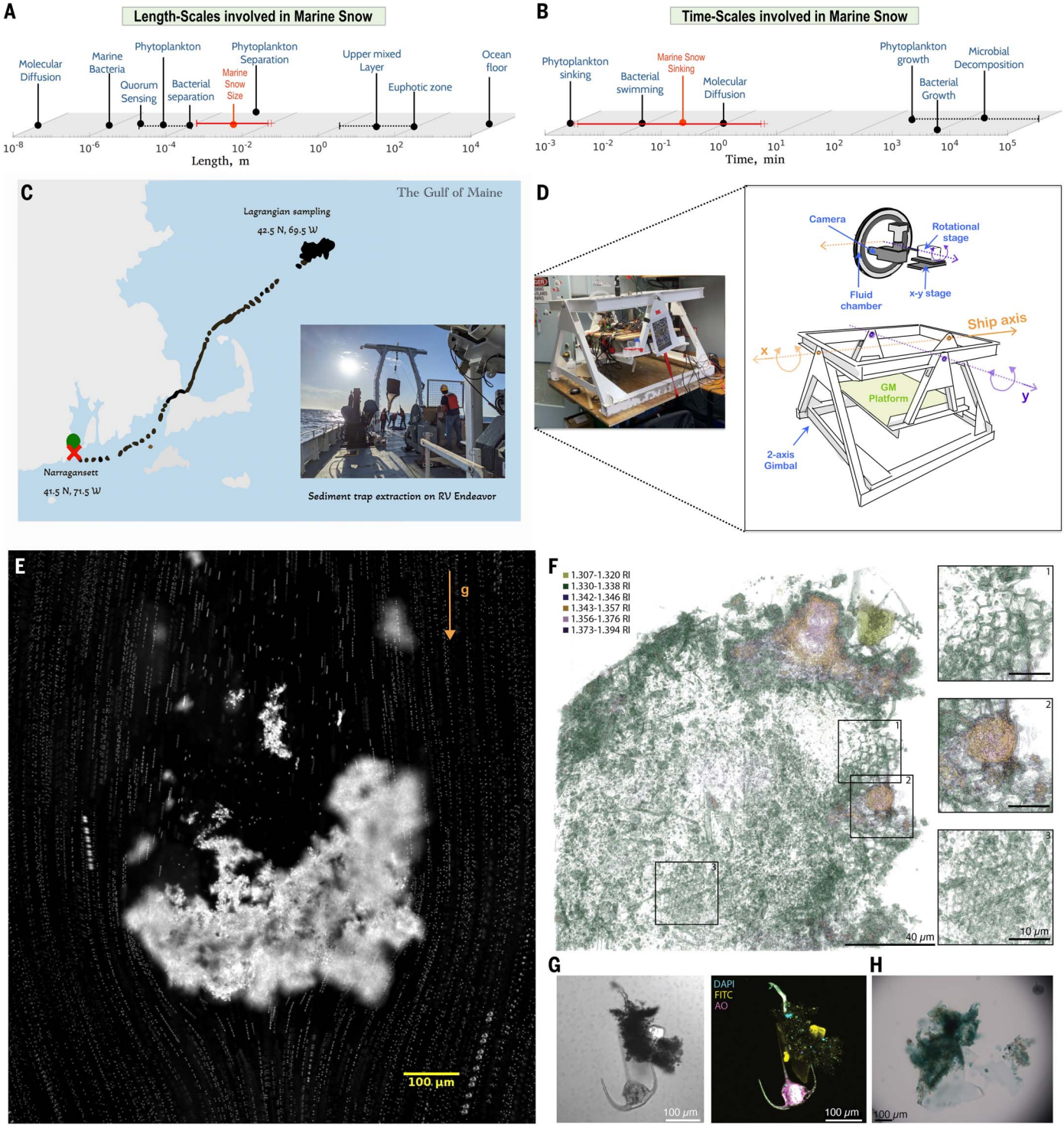

Fig. 1. Marine snow sedimentation in a field setting. (**A** and **B**) Depiction of the multiple length and timescales spanning the biological pump based on previous studies (see supplementary materials). The overall birth, life, and death of "marine snow" exhibits a very broad range of sizes and sedimentation timescales. The timescale of sinking is defined as the time it takes for marine snow to sink by its own body length, based on (*21*). (**C**) Expedition route to the Gulf of Maine and Lagrangian sampling on the map; the inset shows a picture of the sediment trap sampling on RV Endeavor. (**D**) Experimental setup of GM on a mechanical two-axis Gimbal (fig. S2) hanging on RV Endeavor in the open ocean. For details on scale-free vertical tracking microscope (GM), see (*53*). For marine snow experiments, a very wide wheel of 5-mm depth was used for tracking particles that were 700 µm or smaller sinking in the midplane of the GM wheel, ensuring that wall effects were negligible during imaging. (**E**) Flow-trace image of sinking marine snow visualized by using tracer beads ranging from 700 nm to 2 µm. (**F**) A 3D visualization of a marine snow particle made by using holotomography-based imaging (*60*) (Tomocube) of a marine snow aggregate collected at 150 m on RV Endeavor shows the variance of refractive indices (RIs) within a single particle, visualizing frustules of diatoms, radiolarians, and dinoflagellates. (**G**) A representative bright-field and confocal image of a marine snow particle picked from a larger dataset imaged with confocal microscopy (fig. S5). High-resolution

imaging clearly reveals inhomogeneous and biotic origins of marine snow as depicted in both bright-field and confocal images, where an embedded dinoflagellate can also be seen. The DAPI, FITC, and AO channels all emit signal visible from the autofluorescence of the particle. *g*, acceleration due to gravity. (**H**) Alcian blue staining of marine snow from an 80-m sediment trap to visualize TEPs as a representation of polysaccharides present in the marine snow particles. The alcian blue stain is visible throughout the particle. A larger dataset of confocal images for particles is included in the supplementary materials.

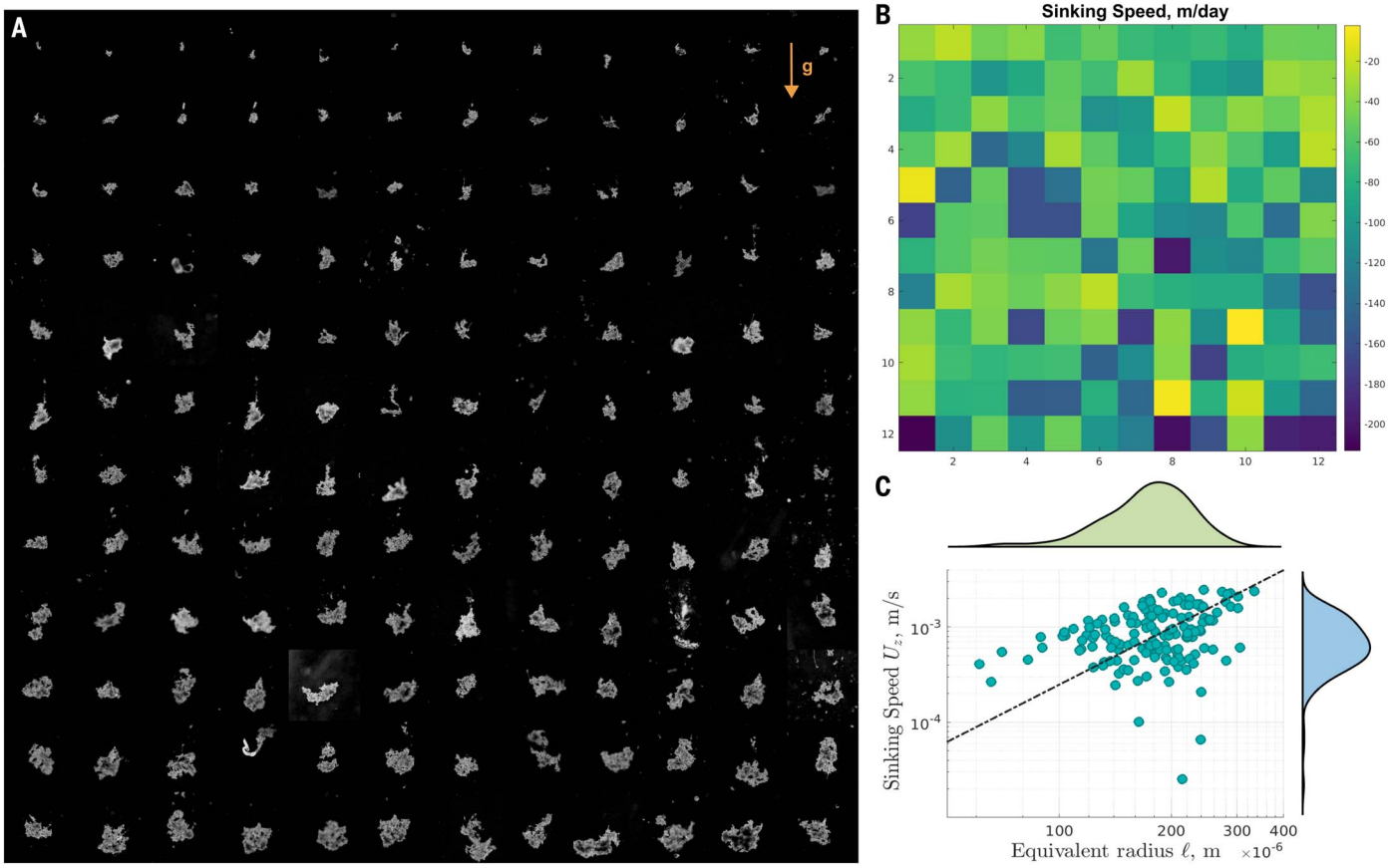

Fig. 2. The plethora of sinking aggregates. (**A**) The collage (12 × 12) of aggregates in their stable sinking configuration. Each image represents a live sedimentation dynamics dataset of an individual particle. For example, the aggregate in Fig. 1E corresponds to (row, column) = (9, 5). Each image panel is 1.27 × 1.27 mm^2. (**B**) Direct measurement of sinking velocity corresponding to every particle in (A), where each (row, column) in (B) corresponds to the same in (A), with a color bar ranging from deep blue (200 m/day) to yellow (0 m/day). (**C**) A log-log plot of sinking speed U_z as a function of equivalent radius ℓ (circle with the same projected area as that of the particle) with a kernel density of ℓ (green) and U_z (blue). The dotted line represents the Stokes' law fit ($U_z \sim l^2$) with a constant effective density ρ_{SW} + 11.4 kg/m^3, depicting a lack of deterministic Stokes' trend, as seen in the spread of the data. Fitting a normal distribution on the particulate aggregate sizes gives a mean of μ = 187.35 ± 8 μm and a standard deviation of σ = 51.93 ± 6 μm.

sedimentation of these heterogeneous multiphase particles and predict the associated elastic modulus of the mucus, relative density of these particles, and overall residence time in a relatively calm water column. Notably, this mucus-based impedance nearly doubles the residence time of marine snow aggregates in the upper productive layer of the ocean, potentially facilitating rapid remineralization by microbes and zooplankton (*8*, *40*, *53*, *54*).

Results

Field observations

To study the sedimentation of fresh marine snow aggregates in a field setting, we went on an expedition on the RV Endeavor in the Gulf of Maine (Fig. 1C) from 12 to 22 June 2021 (RIPPLE Cruise ID: EN667). Marine snow aggregates were collected in multiple deployments of freely hanging sediment traps that had a diameter of 2 m and a mesh size of 50 μm (*13*, *51*) around 42.5°N 69.5°W at a depth of 80 m for a duration of 24 hours. The chlorophyll map of the region indicated the occurrence of a bloom, and thus, these particles were organic-rich, primarily originating from phytoplankton. We also measured particulate organic carbon (POC) fluxes from PIT traps, primary production from ^{13}C arrays, POC concentrations in primary production arrays, and core CTD casts using methods described in (*13*) quantifying the export dynamics (see supplementary materials).

The marine snow samples collected in the sediment trap were brought to the surface and divided by using a quantitative splitter (*55*) into 12 individual bottles. To keep marine snow alive and active, we always kept the samples at the in situ temperature. Individual particles collected from the sediment traps were carefully introduced into the GM wheels (*52*) to avoid any appreciable shear on the particles (Fig. 1D). Microscale sedimentation dynamics of marine snow particles were imaged within hours after the samples were brought to the

ship. These experiments became challenging at high seas owing to the ship frame of reference rocking and rolling. These perturbations were canceled by mounting the imaging system inside a custom-built two-axis gimbal (Fig. 1 D and movie S1).

Imaging individual particles by gently adding them to the imaging wheel allowed us to focus on the response of marine snow to the self-generated hydrodynamic stresses due to gravitational sinking (*56*). This allowed us to study the mechanical response of a sinking aggregate, its detailed fluid-structure interaction, and its rich composition. In these measurements, we ensured a dilute limit such that interparticle hydrodynamic interactions (*39*) can be neglected. Marine snow aggregates are delicate, and thus, their sampling presents a customary challenge (*21*). To examine the possibility of any noteworthy structural disruption or compaction of our marine snow sample while handling (*8*), we compared the fractal dimensions and size-sinking statistics (see supplementary materials) with previous in situ measurements, which ruled out this possibility (*57*). The essential outcomes of our study are, however, not sensitive to these structural details, provided that the composition of our marine snow sample reflects its native in situ character. We ensured this by gently handling the sampled aggregates and making our measurements immediately after the sediment trap retrieval.

In this new GM-based sedimentation assay, we directly measured the settling velocity by tracking individual particles while simultaneously performing high-resolution imaging of marine snow (Fig. 1E). We visualized the microhydrodynamic flows around marine snow by adding polystyrene beads with diameter ranging from 700 nm to 2 μm, yielding high-resolution PIV data. This enabled us to acquire a one-to-one map between structure, flow morphology, and sedimentation velocity of marine snow, which we present in the following sections.

Heterogeneous microstructure of marine snow

Limited volumetric imaging has previously been performed on marine snow particles (*58*). To better understand the three-dimensional (3D) microstructure of a marine snow particles, we performed the first quantitative phase imaging (holotomography) in 3D and obtained isolated materials based on refractive index (Fig. 3A). This method allowed us to observe the heterogeneity in the density of samples without fixation or stains (*59*). The heterogeneous structure was clearly depicted, highlighting segments of diatom and radiolarian frustules embedded in the marine snow particle as ballast (Fig. 3A and movie S3). Next, we imaged particles using bright-field and confocal microscopy (Fig. 3B and fig. S5) to observe the presence of biological materials within the sample. Upon labeling the particles with 4′,6-diamidino-2-phenylindole (DAPI), fluorescein isothiocyanate (FITC), and acridine orange (AO) stains, individual planktonic and bacterial cells embedded in marine snow could

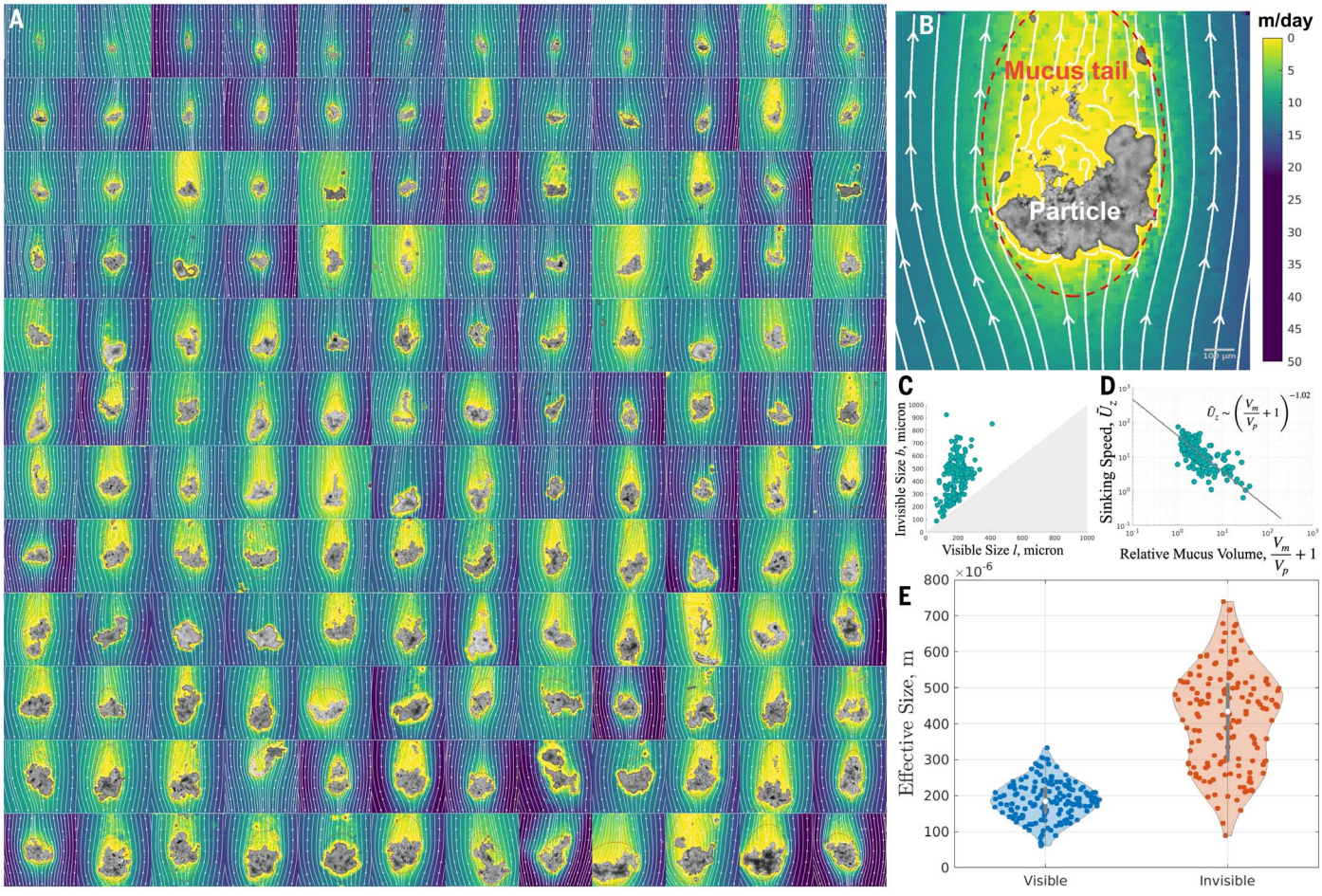

Fig. 3. Hydrodynamic signature of marine snow. (**A**) PIV images showing the hydrodynamic signature of the marine snow, making visible the mucus comet tails. (**B**) Mucus tail around the visible aggregate (row, column) = (9, 5), the same aggregate as in Fig. 1E. (**C**) The visible component of marine snow plotted against the invisible mucus degree of freedom. (**D**) Nondimensional sinking speed (Eq. 5) plotted against the relative mucus volume V_m/V_p shows a systematic decrease in sinking speeds as a function of mucus volume with an exponent ≃−1. (**E**) The violin plot of the invisible size of marine snow (red) compared with the distribution of the visible size spectrum (blue). Accounting for the mucus gives the mean size μ_m = 415.1 ± 21 μm and standard deviation σ_m = 136.3 ± 15 μm (see Fig. 2C for comparison).

be distinctly visualized. Lastly, we imaged with a color camera and bright-field imaging after staining particles with alcian blue to directly visualize TEPs as a representation of polysaccharides present in the marine snow particles (Fig. 3C). Through the combination of these three imaging datasets, we were able to delineate the heterogeneous presence of biotic material, ranging from whole cells (Fig. 3B) to fractions of whole cells, both rigid in diatom frustules (Fig. 1D) and soft in mucus (Fig. 1, E and F). Although imaging of stationary particles under a confinement such as a glass slide does not correlate to the actual configuration of a sinking particle, we were still able to build a comprehensive picture of the microscopic components present in a marine snow particle. The associated datasets highlight its rich composition and heterogeneous distribution of density across the many particles that we imaged. To build reduced-order models, we defined the particulate density ρ_p as an average over this underlying distribution, and the density of the TEP or mucus is represented as ρ_m.

Direct measurement of sedimentation dynamics

Imaging free-falling marine snow aggregates (Fig. 1E) highlights the complex geometry of these particle that are soft and deformable owing to self-stress from sedimentation. 3D tomography revealed (Fig. 1F) a highly heterogeneous density distribution for the aggregates. Understanding how each of these aspects couple together and ultimately results in sinking speed and to precisely determine the density-to-drag ratio (*35*) necessitates independent in situ measurements of individual particles (*22*). Thus, we comprehensively investigated the sinking dynamics of all collected particles while on board the ship by tracking individual marine snow aggregates in the GM (*52*). Hydrodynamic levitation and tracking coupled to high resolution imaging (0.828 μm resolution at 5 fps) allowed us to directly measure the sinking speed of individual particles while simultaneously capturing detailed structure of every aggregate. Microscopy in an untethered state of forever-sinking particles yielded high-resolution images, presented as a collage of aggregate shapes and sizes (Fig. 2A), where gravitational torques owing to shape polarity have already aligned to the principal axis of the aggregate along gravity (*60*). This resulted in a nearly stable sedimentation orientation over the measurement window of ≃5 min. Fractal analysis of these shapes in their sinking state gave the 2D fractal dimension D_2 = 1.6516 ± 0.0745 (fig. S4D), which is in the same range as that reported previously for in situ particles (*35*, *49*). Furthermore, particle tracking produced a one-to-one map between detailed structure of marine snow (Fig. 2 A) and sedimentation velocity (Fig. 2 B), with velocities ranging widely between 5 and 200 m/day.

The Reynolds numbers (*Re*) associated with each sampled particle was <1 (see supplementary materials), rendering inertia negligible. We estimated the equivalent spherical radius ℓ of these aggregates by image thresholding (*61*) (see supplementary materials), where a visible spectrum of aggregate "radius" imaged ranged between 50 and 350 μm, with mean radius 187.35 ± 8 μm (Fig. 2C). Plotting sinking speeds U_z as a function of equivalent spherical radius ℓ showed a significant variability in the sinking velocity for the same size, presenting the lack of a deterministic Stokes trend (*38*) in the size-sinking plane (Fig. 2C). This discrepancy has been noted previously for larger aggregates in classic marine snow studies (*62*). This variability in the density-to-drag ratio (*35*) has been previously treated statistically (*18*), and empirical prescriptions have been developed for incorporating this through fractal geometry (*48*). But the underlying sedimentation physics that give rise to this discrepancy remain poorly understood. In our observations, we occasionally also encountered unsteady singular events, such as merging, fracture, slow depletion owing to hydrodynamic stresses, and grazing by ciliates and copepod (*40*), all of which add further richness to marine snow sedimentation and likely make it a highly dynamic process at long-settling timescales, which we did not pursue in this investigation.

Observed uncertainty in the density-to-drag ratio across particles (Fig. 2C), even within the same marine snow type, can be attributed to variability in the internal degrees of freedom of marine snow, such as shape, density, and TEP. To further scrutinize these hidden degrees of freedom, we examined the fluid dynamics around individual sinking aggregates. In the following sections, based on PIV measurements, we lifted the classic size-sinking relationship to a higher dimensional space of structure (size and shape) and material property (elasticity, viscosity, and density), all of which together determine the mobility tensor (*60*) and buoyancy of marine snow.

Invisible comets of mucus

Studies with fluidized bed geometry (*63*, *64*) and microfluidic channel (*43*) have previously shed light on the flows around field-collected and artificial aggregates generated in a lab setting. But the environment on a research vessel presents a notoriously challenging venue for measuring these delicate microscale flows, as the flow signal in consecutive images laden with PIV beads is nested in the background noise coming from both the high-frequency jitters and the canonical rock and roll dynamics of the ship. These noise sources depend on the stability of the vessel and the ocean conditions. To mitigate roll and pitch of the boat, we mounted the vertical tracking microscope (GM) (*52*) on a passive two-axis gimbal (Fig. 1D) to suppress the low-frequency tilt noise. The high-frequency jitter noise was removed through cushions and in a custom-designed image-processing pipeline (see supplementary materials). The resultant microscale PIV of individual marine snow aggregates (Fig. 3A) and direct measurement of the sinking velocities (Fig. 2D) with an unprecedented resolution for a field setting. Beads could be clearly seen to flow around the sinking particles, marking the flow field precisely. Notably, the measured flow field around these sinking aggregates conspicuously displayed a transparent mucus comet tail behind the particles, highlighted as a region of zero velocity (yellow region, Fig. 3B, and movie S2). The aggregate in Fig. 3B is the same as in Fig. 1E, with its "hidden" viscoelastic degrees of freedom now made visible through PIV analysis. Staining of particles (Fig. 1H) confirmed that mucus (TEP) was present on our particles and is of biological origin (*16*, *44*).

The visualization of comet-like morphology of the mucus around marine snow aggregates, a hitherto-unknown feature, was universal across all particle shape and sizes (Fig. 3A) in this dataset. We note that these transparent extensions of marine snow endow a "comet" [a term coined in (*22*)] with a mucus tail, which bears a superficial resemblance to the plumes resulting from advection and diffusion of chemicals around sinking marine aggregates (*43*, *65*–*68*). However, the gel-like polymer nature (*44*) of mucus tails makes them physically distinct in their dynamical response and in their influence on sedimentation dynamics. Whereas a chemical trail does not impact the sedimentation physics, a "physical" mucus tail significantly reduces the sedimentation velocity because of the drag and buoyancy associated with these tails, bringing some of the marine snow particles to a near standstill, which we elucidate below.

To proceed, we quantified the amount of mucus that an aggregate is dressed in by measuring the length of the semimajor and semiminor axes of the mucus comet, defined as b and a, respectively. The tail length (b) was found to be weakly positively correlated with the size of the visible aggregate, ℓ (Fig. 3C) (see supplementary materials). The relation between ℓ and b depends on both the natural history of a particular marine snow particle, involving the convoluted nature of aggregation dynamics (*16*) and the microhydrodynamics of marine snow itself. For these soft and delicate aggregates, morphology determined sinking and hydrodynamic stresses owing to sinking in turn sculpting the morphology. This two-way coupling is a key dynamical aspect of marine snow, which manifests only in untethered measurements.

To investigate how mucus tails modify sinking dynamics, we measured the mucus volume ($V_m \sim a^2 b$), volume of the visible particle

($V_p \sim \ell^3$), and the sinking speed U_z simultaneously. We defined a nondimensional velocity $\tilde{U}_z \equiv U_z T/a_0$ using length scale a_0 defined as the radius of a sphere with volume $V = V_m + V_p$ as well as the sedimentation timescale $T = 9\mu/2g(\rho_{sw} - \rho_m)a_0$, where ρ_m and ρ_p are mucus and particulate density, respectively, as defined previously, and ρ_{sw} is the density of the sea water such that $\rho_{sw} \neq \rho_m$. Figure 3D shows that the relative volume of mucus V_m/V is inversely proportional to the settling velocity $\tilde{U}_z$.

We found that the invisible size spectrum of marine snow was dramatically distinct from the visible size spectrum (Fig. 2C), with mean b = 415 ± 21 μm being more than twice the mean visible size ℓ. The presence of this additional mucus phase introduces a completely new fluid mechanical boundary condition, which radically modifies the effective size of marine snow and presents a multiphase fluid-structure interaction problem. Notably, we did not observe any appreciable flow through the aggregates (Fig. 3A) even when they appeared to be visibly porous, which is likely because mucus suppresses the permeability of marine snow by clogging the pores. Because the mucus density ρ_m was less than ρ_p, increase in relative mucus volume also led to increase in buoyancy. The observed reduction in sinking speed is a natural consequence of increase in effective buoyancy owing to lower density and simultaneous increase in hydrodynamic resistance owing to the prescence of an extended mucus comet tails.

Two-phase model of marine snow dressed in mucus

To contextualize our experimental observations in the framework of Stokesian sedimentation while seeking closed-form analytical expressions for the buoyancy and hydrodynamic resistance, we turned to the basic building blocks of this distinct dynamical system. We treated marine snow as a two-phase aggregate with visible particulate aggregate embedded in the invisible mucus halo, sedimenting under its own weight. Hydrodynamic self-stress generated owing to sedimentation elongates the shape of mucus halo, which in turn modifies the sinking speed, further changing the sedimentation self-stress. This key feedback mechanism determines the steady-state shape and sinking velocity of these particles. We incorporated this two-way coupling between deformation and sedimentation into our minimal model and elucidated the microphysics of marine snow sedimentation. Our goal here is to capture the essential physics while still being general enough for the essential physics to be applicable to a broad range of marine snow particles. Based on our field observations of freshly collected marine snow aggregates, we constructed a minimal model for the Stokesian sinking of marine snow with mucus halo by analytically treating the halos as a deformable prolate spheroid (*69*) with semimajor and semiminor axes b and a, respectively, and density ρ_m. With mean Reynolds number Re = 0.19 ± 0.02 (see supplementary materials) significantly <1, we neglected particle inertia (*70*, *71*). The visible particulate aggregate with effective radius l has a density ρ_p (particle) greater than ρ_m (mucus) (Fig. 4A).

Because the particulate matter is at the bottom of the mucus halo and $\rho_m < \rho_p$, marine snow with mucus halo is effectively a bottom-heavy sedimenting particle (*72*, *73*). In the ambit of linear response, the shape degree of freedom $\delta\boldsymbol{b} \equiv (b/b_0 - 1)\hat{z}$ is assumed to evolve viscoelastically through the Kelvin-Voigt (KV) model (*74*), and the translational degree of freedom $\mathbf{X}$ is governed by the Stokesian mobility relation (*75*, *76*) $\mathrm{M}(\delta\boldsymbol{b})$ (*60*, *69*), giving rise to the coupled equations for shape and sinking dynamics, respectively:

$$\dot{\delta\boldsymbol{b}} + \frac{E}{\mu}\delta\boldsymbol{b} = \frac{\alpha}{\mu'}\boldsymbol{\sigma}\cdot\boldsymbol{b} \tag{1}$$

$$\dot{\boldsymbol{X}} = M(\delta\boldsymbol{b})\cdot\boldsymbol{F} \tag{2}$$

In Eq. 1, $\boldsymbol{\sigma} = (\nabla v + \nabla v^{\mathrm{T}})/2$ is the symmetric part of the velocity gradient generated by a force monopole of strength $\mathbf{F}$, which is assumed to be located at the origin of visible particulate aggregate, due to its relatively dominant contribution to weight as compared to mucus (*77*). $\mathbf{F}$ induces translational dynamics of the center of gravity $\mathbf{X}$ of marine snow through the mobility relation (Eq. 2). In Eq. 1, the second term on the left captures the viscoelastic relaxation, and the term on the right presents a one-way hydrodynamic coupling between the KV dimer located at the origin of mucus halo and sedimentation induced flow v to leading orders in velocity gradient. The phenomenological parameter α can, in general, depend on the shape of the viscoelastic halo, and determining it requires solving the boundary-value problem (*78*, *79*). For the sake of simplicity in the present analysis, we fix $\alpha = \mu$ on dimensional grounds. When the extensional axis is aligned with the gravity axis, thanks to the polarity of the marine snow, the Stokesian hydrodynamic stress induced by $\mathbf{F}$ along $\mathbf{b}$ to leading order in l/a_0 becomes (see supplementary text):

$$\boldsymbol{\sigma}\cdot\boldsymbol{b} = \frac{2}{3}\frac{a_0(\rho_{sw} - \rho_m)\boldsymbol{g}}{(1+\delta\boldsymbol{b})^2}\left(\frac{V_p}{V}\tilde{\rho} - 1\right) \tag{3}$$

We have defined $\tilde{\rho} \equiv (\rho_p - \rho_m)/(\rho_{sw} - \rho_m)$, which lumps the sea water density ρ_{sw}, mucus density ρ_m, and aggregate density ρ_p into a single nondimensional density parameter. We consider a volume conserving mucus and an isotropic initial condition with nonzero mucus volume, $b_0 = a_0 > \ell$. Combining Eqs. 1 and 3 and nondimensionalizing Eqs. 1 and 2 using length scale a_0 and sedimentation time scale $T = 9\mu/2g(\rho_{sw} - \rho_m)a_0$ for $\rho_m \neq \rho_{sw}$ gives the dynamical equations for longitudinal deformation δb and vertical depth z scaled by a_0,

$$\dot{\delta b} + \frac{\mu}{\mu'}D\delta b = 3\frac{\mu}{\mu'}\left(\frac{V_p}{V}\tilde{\rho} - 1\right)\frac{1}{(1+\delta b)^2} \tag{4}$$

$$\dot{z} = \left(\frac{V_p}{V}\tilde{\rho} - 1\right)\frac{\mathbb{X}^{-1}(e)}{1+\delta b} \tag{5}$$

In Eq. 1, $D \equiv 9E/[2g(\rho_{sw} - \rho_m)a_0]$ is the ratio of elastic to hydrodynamic stress response, the magnitude of which is set by the biology of mucus secretion in phytoplankton (*44*, *47*, *80*). The scalar mobility of the spheroid with its symmetry axis aligned with gravity, $\mathbb{X}^{-1}(e) \equiv 3[(1+e^2)\ln(1+e/1-e) - 2e]/8e^3$, captures shape-dependent sinking as a function of eccentricity $e = \sqrt{1-(1+\delta b)^{-3}}$. Eq. 5 gives the condition for nonzero sinking of the marine snow $V_m < V_p(\tilde{\rho} - 1)$, implying that marine snow with larger mucus halos falls slower, allowing for the possibility of neutral and even negative buoyancy depending on the amount of mucus. This striking role of mucus in suppressing drift potentially reduces the net carbon flux in the ocean (*44*), bringing some of the aggregates to a near stand-still (Fig. 2).

We solved Eqs. 4 and 5 in the steady-state approximation of the mucus comet tail δb = 0, where the viscosity sets the timescale to achieve the steady state; however, the steady-state solution is independent of μ and μ'. A stable fixed point is guaranteed in Eq. 4, and the steady-state tail length has a closed-form expression (see supplementary materials), which is plotted as a function of D, V_p/V, and $\tilde{\rho}$ (Fig. 3B). Asymptotic analysis of the steady state yielded two scaling regimes, one for very small and one for very large deformations (see supplementary materials). Figure 4C shows the steady-state sinking velocity (Eq. 5) as a function of D, V_p/V, and $\tilde{\rho}$.

Viscoelastic rheology of xanthan gum in salt solutions has provided useful insights into the hydrodynamic nature of marine mucus, whereas in situ measurements remain limited (*81*, *82*). We present a "sedimentation-based" measurement of the susceptibility of fresh marine snow mucus in a field setting (*44*). Comparison between theory and field data allowed us to get the density distribution of the visible particulate matter (Fig. 4D), which further enables this sedimentation-based measurement of the elastic modulus of mucus (see supplementary materials), with the mean value of 0.028 Pa (Fig. 4E).

Our field experiments and theoretical framework show that the sinking speed of a two-phase

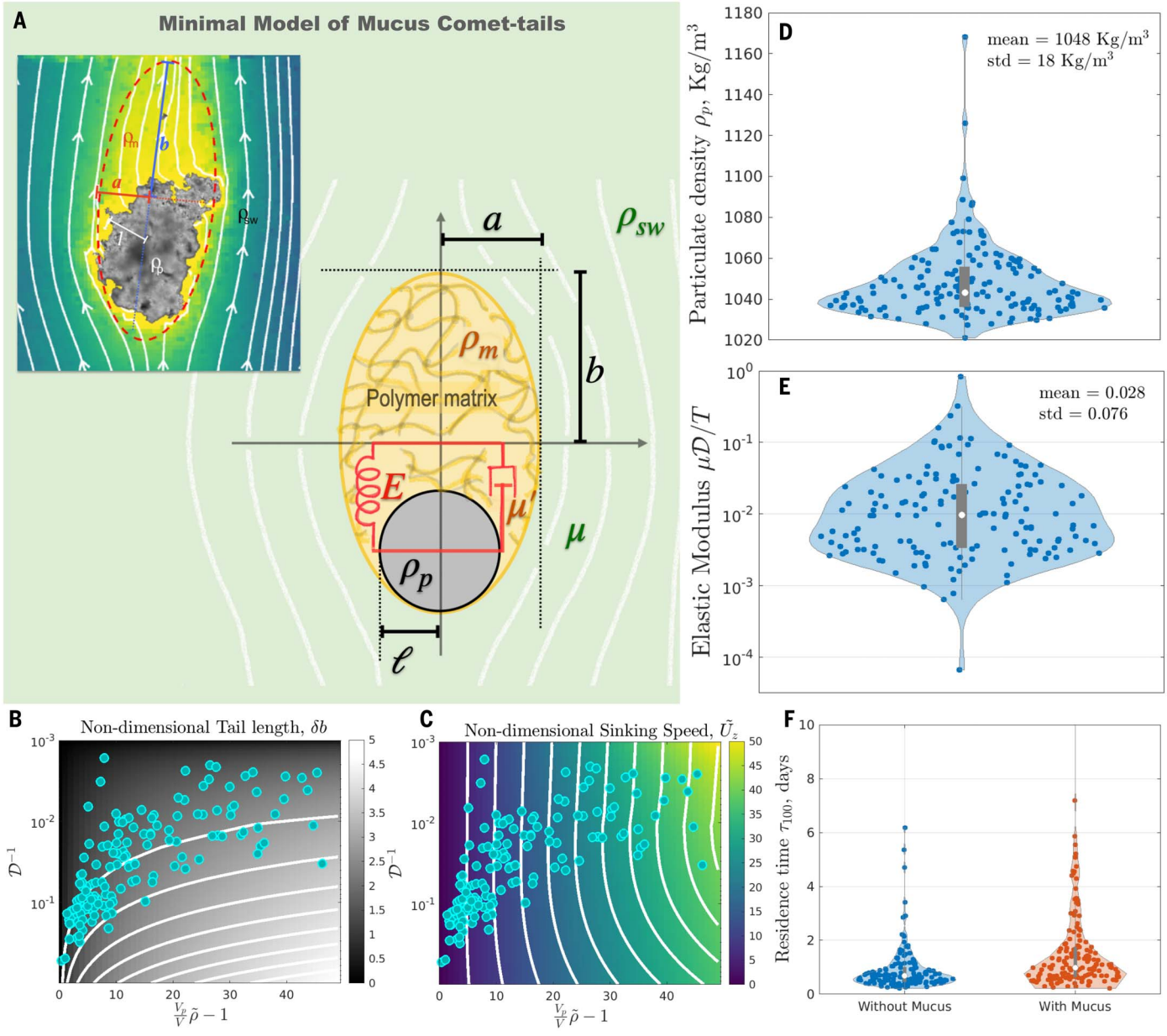

Fig. 4. Two-phase model and sedimentation-based rheology of marine snow. (**A**) The inset shows measured flow field around a sinking particle corresponding to (row, column) = (8, 3) in Fig. 2D. Schematic of the reduced-order model with an approximately prolate-spheroidal mucus halo enclosing the visible particulate aggregate with the various densities ρ_m, ρ_p, and ρ_{sw} and length scales semiminor axis *a*, semimajor axis *b*, and equivalent spherical radius ℓ in the mucus comet tail marked. The viscoelastic degrees of freedom of mucus are lumped into an elastic modulus *E* and a viscous modulus μ' that is different from the viscosity of sea water μ. (**B**) The steady-state solution of Eq. 4 gives the mucus tail length δb as a function of the internal structural degrees of freedom of marine snow $(V_p/V, \tilde{\rho}, \mathcal{D})$. White curves represent the contours of constant tail length. (**C**) The steady-state solution of Eq. 5 gives the vertical sinking speed as a function of $(V_p/V, \tilde{\rho}, \mathcal{D})$. White curves represent constant speed contours. (**D**) The corrected distribution for particulate density after accounting for the mucus. Std, standard deviation. (**E**) The distribution of the elastic modulus of the mucus in pascals by measuring the distortion and sinking speed, presenting a sedimentation-based rheology. (**F**) The residence time distribution of marine snow in upper the 100 m of the ocean for cases with (red) and without mucus (blue) (see supplementary materials).

particle is inversely proportional to the relative volume of mucus in marine snow (Fig. 3D), which is in accord with Eq. 5. This mucus-induced impedance in marine snow reduces the sedimentation flux and increases the residence time of mucus-rich aggregates in our dataset. The estimate of residence time shows that the presence of mucus almost doubled the mean residence time of marine snow in the upper 100 m of the ocean (1.92 days) compared with that without mucus (0.9 days) (Fig. 4F and supplementary materials), assuming a steady sinking state. Such a notable increase in residence time in the water column would greatly impact the total downward flux due to bacterial degradation (*8*, *42*, *54*).

Summary and future challenges

Advances in our understanding of open ocean ecosystems and of marine snow in particular has historically developed in tandem with advances in marine technology. Our study uses implementation of scale-free vertical tracking microscopy in a field setting, a recent technological development (*52*), to shed light on the

essential dynamical aspects of marine snow sedimentation. To the best of our knowledge, we present the first microscopic window into the sedimentation physics of these complex multiphase soft-matter particles and highlight the consequences on carbon export in our oceans. Broadly linking this gravity-based transport phenomena that is governed by microscale parameters to larger-scale ocean carbon flux dynamics (*3*) is crucial for understanding tipping points and balancing the carbon budget in current ocean-based carbon sequestration estimates (*9*).

Our work also presents the largest-known dataset of microscale hydrodynamics of marine snow sedimentation, with more than 100 particles imaged individually. By directly measuring the sinking velocities and detailed flows around individual marine snow particles at sea moments after they are brought on board, this new platform will enable the study of how these particles are transformed by biological activity, such as microbial remineralization, over longer timescales. Our datasets establish a distinct size-sinking dataset in which both the sizes of dense particles and lighter mucus halos are measured independently. Although past studies have measured similar order-of-magnitude numbers (*18*, *33*) (see supplementary materials), such comparisons must be treated cautiously, asthe true "size" of a composite particle should include both visible cellular components and invisible mucus. Broadly, we envision that the new measurement tools presented here will solidify a new standard for in situ sedimentation analysis of marine snow.

The carbon content of TEP is comparable to that of the particulate matter (*83*). TEP production has also been shown to increase linearly with the increase of dissolved carbon dioxide in the ocean (*84*) and in response to both biotic and abiotic stressors in phytoplankton (*47*). Although the presence of mucus has been long known in marine snow particles, past studies have primarily focused on its impact on particle aggregation (*16*, *44*–*46*). Because our work emphasizes the critical role that mucus comet tails can play in reducing the sedimentation velocity of marine snow particles, many factors, including climate change, can have a direct impact on carbon sequestration with the TEP knob (*85*).

Because many of the current estimates of marine snow sedimentation rely on "visible" size distributions, which do not include the mucus layer, our findings, when incorporated with other datasets (*18*, *32*), could help to reconcile discrepancies in flux estimates reported previously (*33*, *34*). We corroborated our findings with 3D volumetric imaging of marine snow particles, which further highlights the heterogeneous nature of marine snow particles and, hence, variation in their density distributions. We have also provided a new theoretical framework based on Stokesian dynamics in which we include this previously invisible degree of freedom and present a modified stokes law for these compound particles. We present a combination of field experiments and theory that also allows us to carry out sedimentation-based rheology of marine snow in the field, enabling estimates of in situ viscoelastic properties of marine snow.

Given the many-particle character of agglomeration of organic matter to form marine snow (*16*), we expect that a probability distribution in (D, V_p/V, $\tilde{\rho}$) parameter space (Fig. 4C) governs the net flux of matter through a horizontal plane in the ocean. A detailed knowledge of this distribution will enable better estimates of carbon flux in the ocean. In future expeditions, we will fill this gap in available data. We believe our approach paves the way to linking microscale in situ observations of marine snow to understanding the macroscale biological pump from the bottom up and bringing marine snow phenomena in the ambit of soft matter physics.

The rapidly changing climate (*86*) necessitates improved observations and predictive understanding of oceanic carbon flux. Our work currently describes the complex sedimentation dynamics of marine snow particles. Combined with mechanisms and rates of marine snow formation and their remineralization by microbes, this framework has the potential to provide a fundamental bottom-up description for 1D flux models, such as the Martin curve (*3*). Currently, it is estimated that 30% of anthropogenic carbon is sequestered by the ocean through biological pump. We observed a 100% increase in the residence time of mucus-heavy marine snow particles, likely facilitating remineralization by microbes and reducing the overall flux that can be sequestered by this mechanism. Given the current uncertainty in biological pump in a changing global climate (*33*), it is imperative to underpin the microbiology and microphysics of marine snow. Our direct in situ and on-vessel field setting measurements of a broad range of marine snow particles provide a promising approach to predictively understanding the biological pump.

Materials and methods

Sample collection

Data was collected while on board the RV Endeavor during the cruise using a GM [for details on the instrument, see (*53*)]. We used freely hanging sediment traps in the Lagrangian mode (*89*) on RIPPLE1 expedition (11 to 23 June), 2021 (Cruise ID: EN667) with mesh size (50 μm) at 80 m depth in the Gulf of Maine on RV Endeavor [design of the net trap used in this study is given in (*52*)]. The nets were recovered after 24 hours (see table S1 for exact times of deployment and recovery). After the cod-end recovery, we passed the material through a quantitative splitter. We used a splitter that is modified from the basic design of (*56*) to accommodate collection of 12 samples instead of 8 and to allow direct electric drive.

Preparing GM wheel

The material collected was gently picked by a wide end pipette and added to a wheel shaped fluid chamber with inner thickness 5 mm. We study particles with equivalent spherical diameter below 750 μm. Thus, ensuring that the wheels are much wider than the particle dimensions, to avoid wall induced shear.

PIV and sedimentation measurement

We mixed 60 μL of 700-nm to 2-μm polystyrene bead solution in 100 mL sea water for doing PIV. We loaded about 1 mL of the sediment from the collected sample in the gravity machine wheel containing the bead sea water solution. After loading the aggregates, the marine snow suspension was gently homogenized by manually rotating the wheel clockwise and counterclockwise multiple times. This homogenization is needed to minimize interparticle hydrodynamic interactions. We then took tracks of marine snow aggregates in GM for around 2 min at 5 fps.

Analysis pipeline

Effective radius and naive Stokesian settling approximation: Gravity machine directly gives the virtual vertical distance traversed as a function of time $z(t)$. The effective vertical position as a function of time, shows fluctuation in vertical velocity due to the ship motion, but this disturbance only adds a residual error in a linear fit, thanks to the gimbal. This gives us the vertical settling speed. To correlate it with the visible particle size we threshold the images after conversion to eight-bit and measure the projected area and from this get the effective radius of a circle with an equivalent area. Comparison of our "visible" size-sinking relationship with the previous in-situ measurement is shown in fig. S3.

Mucus halo measurement: The collected images and tracks were initially processed in a customized ImageJ macro. The vibrations of the ship resulted in misalignment of aggregates in adjacent frames. To remove this noise, we automated the image registration process using a MATLAB script. A command-line based PIV was conducted on the resulting images, on MATLAB PIVLab. The PIV data and GM tracking data were then coherently analyzed for mucus and particulate matter quantification using a custom MATLAB function. All the image processing and analysis were automated.

Alcian blue staining

Particles were stained with alcian blue (AB) to visualize TEP as per previously published protocols (*91*). A stock solution (1% AB in 3% acetic acid in water) was used to prepare a

working solution (0.04% AB). The working solution was then passed through a 0.2 µm pore-size syringe filter prior to staining. Water samples containing marine snow "splits" from the net trap were gently filtered onto 0.4 µm pore-size polycarbonate filters using low and constant vacuum pressure (>200 mbar). Once filtered, 500 µL of the AB working solution was added and the pump was switched on immediately to remove the stain. The filter was then rinsed with 500 µL of double distilled water under gentle vacuum. The filter was then placed in an eppendorf tube with 1.5 mL of 0.2 µm filtered sea water and the sample was agitated to release marine snow particles off of the filter and into the bottom of the eppendorf tube. Samples were visualized immediately and kept at −20°C for additional analyses.

Sample preservation

Particles were preserved in a 4% Paraformaldehyde solution in phosphate-buffered saline solution for 3D structural analysis.

Fluorescence microscopy

Fluorescence microscopy images were collected using a LSM780 Confocal Microscope through the Cell Sciences Imaging Facility at Stanford Univeristy. Samples were mounted in 35 mm glass-bottom petri dishes and were uncompressed. Samples were not stained. Any color present comes from autofluorescence of the particle.

Holotomography

3D refractive index images were collected using holotomography on the Tomocube microscope. Samples were mounted in tomo-dishes and were compressed by 22 × 22 mm coverslips.

REFERENCES AND NOTES

1. T. DeVries, The ocean carbon cycle. *Annu. Rev. Environ. Resour.* **47**, 317–341 (2022). doi: 10.1146/annurev-environ-120920-111307
2. N. Gruber *et al*., The oceanic sink for anthropogenic CO_2 from 1994 to 2007. *Science* **363**, 1193–1199 (2019). doi: 10.1126/science.aau5153; pmid: 30872519
3. J. H. Martin, G. A. Knauer, D. M. Karl, W. W. Broenkow, Vertex: Carbon cycling in the northeast pacific. *Deep-Sea Res. A, Oceanogr. Res. Pap.* **34**, 267–285 (1987). doi: 10.1016/0198-0149(87)90086-0
4. P. Martin *et al*., Export and mesopelagic particle flux during a north atlantic spring diatom bloom. *Deep Sea Res. Part I Oceanogr. Res. Pap.* **58**, 338–349 (2011). doi: 10.1016/j.dsr.2011.01.006
5. H. Ducklow, D. Steinberg, K. Buesseler, Upper ocean carbon export and the biological pump. *Oceanogr.* **14**, 50–58 (2001). doi: 10.5670/oceanog.2001.06
6. M. R. Stukel *et al*., Carbon sequestration by multiple biological pump pathways in a coastal upwelling biome. *Nat. Commun.* **14**, 2024 (2023). doi: 10.1038/s41467-023-37771-8; pmid: 37041189
7. C. De La Rocha, U. Passow, "8.4 - The Biological Pump," in *Treatise on Geochemistry*, H. D. Holland, K. K. Turekian, Eds. (Oxford Elsevier, ed. 2, 2014), pp. 93–122. doi: 10.1016/B978-0-08-095975-7.00604-5
8. A. L. Alldredge, M. W. Silver, Characteristics, dynamics and significance of marine snow. *Prog. Oceanogr.* **20**, 41–82 (1988). doi: 10.1016/0079-6611(88)90053-5
9. P. W. Boyd, H. Claustre, M. Levy, D. A. Siegel, T. Weber, Multi-faceted particle pumps drive carbon sequestration in the ocean. *Nature* **568**, 327–335 (2019). doi: 10.1038/s41586-019-1098-2; pmid: 30996317
10. M. M. Omand, R. Govindarajan, J. He, A. Mahadevan, Sinking flux of particulate organic matter in the oceans: Sensitivity to particle characteristics. *Sci. Rep.* **10**, 5582 (2020). doi: 10.1038/s41598-020-60424-5; pmid: 32221314
11. R. Carson, *The sea around us* (Oxford Univ. Press, 2003).
12. M. Silver, Marine snow: A brief historical sketch. *Limnol. Oceanogr. Bull.* **24**, 5–10 (2015). doi: 10.1002/lob.10005
13. J. R. Collins *et al*., The multiple fates of sinking particles in the north atlantic ocean. *Global Biogeochem. Cycles* **29**, 1471–1494 (2015). doi: 10.1002/2014GB005037
14. D. M. Sigman, E. A. Boyle, Glacial/interglacial variations in atmospheric carbon dioxide. *Nature* **407**, 859–869 (2000). doi: 10.1038/35038000; pmid: 11057657
15. B. N. Cruz, S. Brozak, S. Neuer, Microscopy and dna-based characterization of sinking particles at the bermuda atlantic time-series study station point to zooplankton mediation of particle flux. *Limnol. Oceanogr.* **66**, 3697–3713 (2021). doi: 10.1002/lno.11910
16. A. B. Burd, G. A. Jackson, Particle aggregation. *Annu. Rev. Mar. Sci.* **1**, 65–90 (2009). doi: 10.1146/annurev.marine.010908.163904; pmid: 21141030
17. R. Sanders *et al*., The biological carbon pump in the north atlantic. *Prog. Oceanogr.* **129**, 200–218 (2014) doi: 10.1016/j.pocean.2014.05.005
18. B. B. Cael, E. L. Cavan, G. L. Britten, Reconciling the size dependence of marine particle sinking speed. *Geophys. Res. Lett.* **48**, e2020GL091771 (2021). doi: 10.1029/2020GL091771
19. I. Kriest, A. Oschlies, On the treatment of particulate organic matter sinking in large-scale models of marine biogeo- chemical cycles. *Biogeosciences* **5**, 55–72 (2008). doi: 10.5194/bg-5-55-2008
20. S. A. Henson *et al*., Uncertain response of ocean biological carbon export in a changing world. *Nat. Geosci.* **15**, 248–254 (2022). doi: 10.1038/s41561-022-00927-0
21. R. Lampitt, "Marine snow" in *Encyclopedia of Ocean Sciences*, J. K. Cochran, H. J. Bokuniewicz, P. L. Yager, Eds. (Oxford Academic Press, ed. 3, 2001), pp. 160–169. doi: 10.1016/B978-0-12-813081-0.00218-4
22. A. L. Alldredge, C. Gotschalk, In situ settling behavior of marine snow1. *Limnol. Oceanogr.* **33**, 339–351 (1988). doi: 10.4319/lo.1988.33.3.0339
23. A. Alldredge, C. Gotschalk, Direct observations of the mass flocculation of diatom blooms: Characteristics, settling velocities and formation of diatom aggregates. *Deep-Sea Res. A, Oceanogr. Res. Pap.* **36**, 159–171 (1989). doi: 10.1016/0198-0149(89)90131-3
24. A. L. Shanks, J. D. Trent, Marine snow: Sinking rates and potential role in vertical flux. *Deep-Sea Res. A, Oceanogr. Res. Pap.* **27**, 137–143 (1980). doi: 10.1016/0198-0149(80)90092-8
25. P. S. Hill, J. P. Syvitski, E. A. Cowan, R. D. Powell, In situ observations of floc settling velocities in glacier bay, alaska. *Mar. Geol.* **145**, 85–94 (1998). doi: 10.1016/S0025-3227(97)00109-6
26. M.-P. Jouandet *et al*., Optical imaging of mesopelagic particles indicates deep carbon flux beneath a natural iron-fertilized bloom in the southern ocean. *Limnol. Oceanogr.* **56**, 1130–1140 (2011). doi: 10.4319/lo.2011.56.3.1130
27. E. Trudnowska *et al*., Marine snow morphology illuminates the evolution of phytoplankton blooms and determines their subsequent vertical export. *Nat. Commun.* **12**, 2816 (2021). doi: 10.1038/s41467-021-22994-4; pmid: 33990580
28. N. Nowald *et al*., "In-situ sinking speed measurements of marine snow aggregates acquired with a settling chamber mounted to the Cherokee ROV," OCEANS 2009-EUROPE, 11 to 14 May 2009, Bremen, Germany (IEEE, 2009). doi: 10.1109/OCEANSE.2009.5278186
29. A.-R. Diercks, V. L. Asper, In situ settling speeds of marine snow aggregates below the mixed layer: Black sea and gulf of mexico. *Deep Sea Res. Part I Oceanogr. Res. Pap.* **44**, 385–398 (1997). doi: 10.1016/S0967-0637(96)00104-5
30. A. M. P. McDonnell, K. O. Buesseler, Variability in the average sinking velocity of marine particles. *Limnol. Oceanogr.* **55**, 2085–2096 (2010). doi: 10.4319/lo.2010.55.5.2085
31. M. Picheral *et al*., The Underwater Vision Profiler 5: An advanced instrument for high spatial resolution studies of particle size spectra and zooplankton. *Limnol. Oceanogr. Methods* **8**, 462–473 (2010). doi: 10.4319/lom.2010.8.462
32. J. R. Williams, S. L. C. Giering, In situ particle measurements deemphasize the role of size in governing the sinking velocity of marine particles. *Geophys. Res. Lett.* **49**, GL099563 (2022). doi: 10.1029/2022GL099563; pmid: 36583182
33. J. M. Lauderdale, B. B. Cael, Impact of remineralization profile shape on the air-sea carbon balance. *Geophys. Res. Lett.* **48**, GL091746 (2021). doi: 10.1029/2020GL091746; pmid: 34219838
34. B. B. Cael, K. Bisson, Particle flux parameterizations: Quantitative and mechanistic similarities and differences. *Front. Mar. Sci.* **5**, 395 (2018). doi: 10.3389/fmars.2018.00395
35. E. Laurenceau-Cornec, T. Trull, D. Davies, C. De La Rocha, S. Blain, Phytoplankton morphology controls on marine snow sinking velocity. *Mar. Ecol. Prog. Ser.* **520**, 35–56 (2015). doi: 10.3354/meps11116
36. M. H. Iversen, R. S. Lampitt, Size does not matter after all: No evidence for a size-sinking relationship for marine snow. *Prog. Oceanogr.* **189**, 102445 (2020). doi: 10.1016/j.pocean.2020.102445
37. V. L. Asper, W. G. Deuser, G. A. Knauer, S. E. Lohrenz, Rapid coupling of sinking particle fluxes between surface and deep ocean waters. *Nature* **357**, 670–672 (1992). doi: 10.1038/357670a0
38. G. Stokes, On the Effect of the Internal Friction of Fluids on the Motion of Pendulums. *Transactions of the Cambridge Philosophical Society* **9**, 8 (1851).
39. R. Chajwa, N. Menon, S. Ramaswamy, R. Govindarajan, Waves, algebraic growth, and clumping in sedimenting disk arrays. *Phys. Rev. X* **10**, 041016 (2020). doi: 10.1103/PhysRevX.10.041016
40. F. Lombard, M. Koski, T. Kiørboe, Copepods use chemical trails to find sinking marine snow aggregates. *Limnol. Oceanogr.* **58**, 185–192 (2013). doi: 10.4319/lo.2013.58.1.0185
41. J. T. Turner, Zooplankton fecal pellets, marine snow, phytodetritus and the ocean's biological pump. *Prog. Oceanogr.* **130**, 205–248 (2015). doi: 10.1016/j.pocean.2014.08.005
42. D. R. Brumley *et al*., Cutting through the noise: Bacterial chemotaxis in marine microenvironments. *Front. Mar. Sci.* **7**, 527 (2020). doi: 10.3389/fmars.2020.00527
43. U. Alcolombri *et al*., Sinking enhances the degradation of organic particles by marine bacteria. *Nat. Geosci.* **14**, 775–780 (2021). doi: 10.1038/s41561-021-00817-x
44. U. Passow, Transparent exopolymer particles (tep) in aquatic environments. *Prog. Oceanogr.* **55**, 287–333 (2002). doi: 10.1016/S0079-6611(02)00138-6
45. A. L. Alldredge, U. Passow, B. E. Logan, The abundance and significance of a class of large, transparent organic particles in the ocean. *Deep Sea Res. Part I Oceanogr. Res. Pap.* **40**, 1131–1140 (1993). doi: 10.1016/0967-0637(93)90129-Q
46. C. P. Laber *et al*., Coccolithovirus facilitation of carbon export in the North Atlantic. *Nat. Microbiol.* **3**, 537–547 (2018). doi: 10.1038/s41564-018-0128-4; pmid: 29531367
47. K. D. Bidle, The molecular ecophysiology of programmed cell death in marine phytoplankton. *Annu. Rev. Mar. Sci.* **7**, 341–375 (2015). doi: 10.1146/annurev-marine-010213-135014; pmid: 25251265
48. E. C. Laurenceau-Cornec *et al*., New guidelines for the application of stokes' models to the sinking velocity of marine aggregates. *Limnol. Oceanogr.* **65**, 1264–1285 (2020). doi: 10.1002/lno.11388
49. J. R. Kilps, B. E. Logan, A. L. Alldredge, Fractal dimensions of marine snow determined from image analysis of in situ photographs. *Deep Sea Res. Part I Oceanogr. Res. Pap.* **41**, 1159–1169 (1994). doi: 10.1016/0967-0637(94)90038-8
50. S. L. C. Giering *et al*., Sinking organic particles in the ocean—Flux estimates from in situ optical devices. *Front. Mar. Sci.* **6**, 834 (2020). doi: 10.3389/fmars.2019.00834
51. M. L. Peterson, S. G. Wakeham, C. Lee, M. A. Askea, J. C. Miquel, Novel techniques for collection of sinking particles in the ocean and determining their settling rates. *Limnol. Oceanogr. Methods* **3**, 520–532 (2005). doi: 10.4319/lom.2005.3.520
52. D. Krishnamurthy *et al*., Scale-free vertical tracking microscopy. *Nat. Methods* **17**, 1040–1051 (2020). doi: 10.1038/s41592-020-0924-7; pmid: 32807956
53. K. O. Buesseler, P. W. Boyd, Shedding light on processes that control particle export and flux attenuation in the twilight zone of the open ocean. *Limnol. Oceanogr.* **54**, 1210–1232 (2009). doi: 10.4319/lo.2009.54.4.1210
54. F. A. M. Simon, A. L. Alldredge, F. Azam, Bacterial carbon dynamics on marine snow. *Mar. Ecol. Prog. Ser.* **65**, 205–211 (1990). doi: 10.3354/meps065205
55. C. Lamborg *et al*., The flux of bio- and lithogenic material associated with sinking particles in the mesopelagic "twilight zone" of the northwest and north central pacific ocean. *Deep Sea Res. Part II Top. Stud. Oceanogr.* **55**, 1540–1563 (2008). doi: 10.1016/j.dsr2.2008.04.011
56. S. Ramaswamy, Issues in the statistical mechanics of steady sedimentation. *Adv. Phys.* **50**, 297–341 (2001). doi: 10.1080/00018730110050617
57. B. B. Cael, A. E. White, Sinking versus suspended particle size distributions in the north pacific subtropical gyre. *Geophys. Res. Lett.* **47**, e2020GL087825 (2020). doi: 10.1029/2020GL087825
58. C. M. Flintrop *et al*., Embedding and slicing of intact in situ collected marine snow. *Limnol. Oceanogr. Methods* **16**, 339–355 (2018). doi: 10.1002/lom3.10251

59. Y. Park, C. Depeursinge, G. Popescu, Quantitative phase imaging in biomedicine. *Nat. Photonics* **12**, 578–589 (2018). doi: 10.1038/s41566-018-0253-x
60. T. A. Witten, H. Diamant, A review of shaped colloidal particles in fluids: Anisotropy and chirality. *Rep. Prog. Phys.* **83**, 116601 (2020). doi: 10.1088/1361-6633/abb5c4; pmid: 33135667
61. S. L. C. Giering, B. Hosking, N. Briggs, M. H. Iversen, The interpretation of particle size, shape, and carbon flux of marine particle images is strongly affected by the choice of particle detection algorithm. *Front. Mar. Sci.* **7**, fmars.2020.00564 (2020). doi: 10.3389/fmars.2020.00564
62. K. Azetsu-Scott, B. D. Johnson, Measuring physical characteristics of particles: A new method of simultaneous measurement for size, settling velocity and density of constituent matter. *Deep-Sea Res. A, Oceanogr. Res. Pap.* **39**, 1057–1066 (1992). doi: 10.1016/0198-0149(92)90039-V
63. H. Ploug, B. Jørgensen, A net-jet flow system for mass transfer and microsensor studies of sinking aggregates. *Mar. Ecol. Prog. Ser.* **176**, 279–290 (1999). doi: 10.3354/meps176279
64. H. Ploug, Small-scale oxygen fluxes and remineralization in sinking aggregates. *Limnol. Oceanogr.* **46**, 1624–1631 (2001). doi: 10.4319/lo.2001.46.7.1624
65. T. Kiørboe, H. Ploug, U. H. Thygesen, Fluid motion and solute distribution around sinking aggregates.: I. small-scale fluxes and heterogeneity of nutrients in the pelagic environment. *Mar. Ecol. Prog. Ser.* **211**, 1–13 (2001). doi: 10.3354/meps211001
66. T. Kiørboe, G. A. Jackson, Marine snow, organic solute plumes, and optimal chemosensory behavior of bacteria. *Limnol. Oceanogr.* **46**, 1309–1318 (2001). doi: 10.4319/lo.2001.46.6.1309
67. G. E. Kapellos, H. J. Eberl, N. Kalogerakis, P. S. Doyle, C. A. Paraskeva, Impact of microbial uptake on the nutrient plume around marine organic particles: High-resolution numerical analysis. *Microorganisms* **10**, 2020 (2022). doi: 10.3390/microorganisms10102020; pmid: 36296296
68. G. A. Jackson, Simulation of bacterial attraction and adhesion to falling particles in an aquatic environment. *Limnol. Oceanogr.* **34**, 514–530 (1989). doi: 10.4319/lo.1989.34.3.0514
69. J. S. McNown, J. Malaika, Effects of particle shape on settling velocity at low reynolds numbers. *Trans. Am. Geophys. Union* **31**, 74–82 (1950). doi: 10.1029/TR031i001p00074
70. E. Loth, Drag of non-spherical solid particles of regular and irregular shape. *Powder Technol.* **182**, 342–353 (2008). doi: 10.1016/j.powtec.2007.06.001
71. S. G. Prasath, V. Vasan, R. Govindarajan, Accurate solution method for the maxey–riley equation, and the effects of basset history. *J. Fluid Mech.* **868**, 428–460 (2019). doi: 10.1017/jfm.2019.194
72. T. Goldfriend, H. Diamant, T. A. Witten, Screening, hyperuniformity, and instability in the sedimentation of irregular objects. *Phys. Rev. Lett.* **118**, 158005 (2017). doi: 10.1103/PhysRevLett.118.158005; pmid: 28452533
73. K. Nissanka, X. Ma, J. C. Burton, Dynamics of mass polar spheroids during sedimentation. *J. Fluid Mech.* **956**, A28 (2023). doi: 10.1017/jfm.2023.32
74. R. M. Christensen, L. B. Freund, Theory of Viscoelasticity, An Introduction, 2nd Edition. *J. Appl. Mech.* **51**, 226–226 (1984). doi: 10.1115/1.3167591
75. J. Happel, H. Brenner, *Low Reynolds number hydrodynamics* (Springer Netherlands, 1983). doi: 10.1007/978-94-009-8352-6
76. S. Kim, S. J. Karrila, *Microhydrodynamics* (Elsevier, 1991).
77. C. Guo *et al*., Distribution and settling regime of transparent exopolymer particles (tep) potentially associated with bio-physical processes in the eastern indian ocean. *J. Geophys. Res. Biogeosci.* **126**, e2020JG005934 (2021). doi: 10.1029/2020JG005934
78. M. Alves, P. Oliveira, F. Pinho, Numerical methods for viscoelastic fluid flows. *Annu. Rev. Fluid Mech.* **53**, 509–541 (2021). doi: 10.1146/annurev-fluid-010719-060107
79. A. Sharma, D. L. Koch, Finite difference method in prolate spheroidal coordinates for freely suspended spheroidal particles in linear flows of viscous and viscoelastic fluids. *J. Comput. Phys.* **495**, 112559 (2023). doi: 10.1016/j.jcp.2023.112559
80. S. Meng, Y. Liu, New insights into transparent exopolymer particles (TEP) formation from precursor materials at various Na+/Ca2+ ratios. *Sci. Rep.* **6**, 19747 (2016). doi: 10.1038/srep19747; pmid: 26790536
81. M. M. Mrokowska, A. Krztoń-Maziopa, M. Dębowski, Effect of exopolymer gels on the viscoelasticity of mucus-rich saltwater and settling dynamics of particles. *Mar. Chem.* **246**, 104163 (2022). doi: 10.1016/j.marchem.2022.104163
82. I. R. Jenkinson, Oceanographic implications of non-newtonian properties found in phytoplankton cultures. *Nature* **323**, 435–437 (1986). doi: 10.1038/323435a0
83. X. Mari, Carbon content and c:n ratio of transparent exopolymeric particles (TEP) produced by bubbling exudates of diatoms. *Mar. Ecol. Prog. Ser.* **183**, 59–71 (1999). doi: 10.3354/meps183059
84. A. Engel, Direct relationship between CO2 uptake and transparent exopolymer particles production in natural phyto- plankton. *J. Plankton Res.* **24**, 49–53 (2002). doi: 10.1093/plankt/24.1.49
85. K. R. Arrigo, Carbon cycle: Marine manipulations. *Nature* **450**, 491–492 (2007). doi: 10.1038/450491a; pmid: 18033286
86. L. Cheng *et al*., Past and future ocean warming. *Nat. Rev. Earth Environ.* **3**, 776–794 (2022). doi: 10.1038/s43017-022-00345-1
87. R. Chajwa, E. Flaum, K. D. Bidle, B. V. Mooy, M. Prakash, Hidden comet-tails of marine snow impede ocean-based carbon sequestration, Dryad (2024); https://doi.org/10.5061/dryad.v15dv4253.

ACKNOWLEDGMENTS

We thank the captain and crew of the RV Endeavor as well as the entire RIPPLE science team, including H. F. Fredricks for her efforts and expertise in marine snow particle capture. We thank all members of the Prakash lab for discussions. We specifically thank the Prakash lab GM team, especially H. Li and D. Krishnamurthy. We thank M. Hannabelle for their technical support during data collection at RIPPLE expedition. We thank the entire GCR research team for their collaborative, interactive and inspiring discussions. **Funding:** R.C. acknowledges support from the International Human Frontier Science Program Organization award LT000704/2021-C and the Stanford Bio-X travel award. E.F. acknowledges NIH grant T32GM008294-29. This work was enabled by a NSF Growing Convergence Research (GCR) grant to K.D.B., B.V.M., and M.P. M.P. further acknowledges financial support from the Schmidt Futures Innovation Fellowship, Moore Foundation, NSF Center for Cellular Construction, Woods Institute for the Environment, NSF GCR award OIA-2020980, and Dalio Philanthropies. **Author contributions:** R.C. and M.P. designed the research with input from K.D.B. and B.V.M. K.D.B. and B.V.M. developed sediment trap sampling techniques and organized the expedition and sampling protocol. M.P., R.C., and E.F. developed custom instrumentation and imaging tools for the expedition. R.C. collected sedimentation dynamics and PIV data. R.C. developed the analysis pipeline and conducted the sedimentation and flow analysis. E.F. processed samples including fixations. E.F. and R.C. did confocal and bright-field imaging of fixed samples. E.F. and M.P. did holotomography. B.V.M. measured the primary production. R.C. and M.P. developed the theoretical model. R.C. and M.P. interpreted the data. R.C. and M.P. wrote the manuscript. **Competing interests:** The authors declare that they have no competing interests. **Data and materials availability:** The data are available in Dryad (*87*). **License information**: Copyright © 2024 the authors, some rights reserved; exclusive licensee American Association for the Advancement of Science. No claim to original US government works. https://www.science.org/about/science-licenses-journal-article-reuse

SUPPLEMENTARY MATERIALS

science.org/doi/10.1126/science.adl5767
Materials and Methods
Supplementary Text
Figs. S1 to S8
Tables S1 and S2
References (*88*–*101*)
Movies S1 to S3

Submitted 25 October 2023; accepted 21 August 2024
10.1126/science.adl5767